Sulfonation of chitosan for enhanced sorption of Li(I) from acidic solutions – Application to metal recovery from waste Li-ion mobile battery

Mohammed Hamza, Hamed Mira, Yuezhou Wei, Salama Aboelenin, Guibal Eric, Waheed Salem

Sulfonation of chitosan for enhanced sorption of Li(I) from acidic solutions – Application to metal recovery from waste Li-ion mobile battery

Mohammed F. Hamza [a,b], Hamed Mira [b], Yuezhou Wei [a,c,*], Salama M. Aboelenin [d], Eric Guibal [e,*], Waheed M. Salem [f]

[a] School of Nuclear Science and Technology, University of South China, Heng Yang 421001, PR China
[b] Nuclear Materials Authority, POB 530, El-Maadi, Cairo, Egypt
[c] School of Nuclear Science and Engineering, Shanghai Jiao Tong University, Shanghai, PR China
[d] Biology Department, Turabah University College, Taif University, Taif, Saudi Arabia
[e] Polymers Composites and Hybrids (PCH), IMT Mines Ales, Alès, France
[f] Medical Labs Department, Faculty of Applied Health Science Technology, Menoufia University, Shebine El-Koam, Egypt

A B S T R A C T

The functionalization of cross-linked chitosan (Chito) by an original sulfonating process allows synthesizing a highly efficient sorbent (Sulfo-C) for Li(I) recovery from acidic solution (at pH ≈2). FTIR and XPS analyses show the main contributions of amine and sulfonic groups in the binding mechanism. Maximum sorption capacity reaches 20 mmol Li g^{-1}, and the sorption isotherms are fitted by the Langmuir Dual Site equation; the process being spontaneous, exothermic and enthalpy-driven. The sorption remains highly efficient in 1 M NaCl solution, while the uptake remains strongly selective in the presence of equimolar concentrations of alkali-earth and heavy elements (Fe > Zn > Mg > Ca > Ni > Al cations). This selectivity ($SC_{Li/Metal}$ varying between 14 and 36) is controlled by the pH (optimum close to 2.2) and slightly increases (up to 16–69) with adding oxalic acid (1% w/ w). The equilibrium is achieved, under selected experimental conditions, within 30–90 min of contact (depending on temperature). Uptake kinetics are fitted by the pseudo-first order rate equation, though the contribution of resistance to intraparticle diffusion cannot be neglected. Bound metal can be completely desorbed using hydrochloric acid solution (0.2 M); the kinetics of desorption is fast (within 20 to 30 min). Both sorption and desorption performances are remarkably stable for 18 cycles (loss in sorption less than 10.4% at the 18th cycle). The functionalized sorbent is highly efficient for the recovery of lithium from a spent Li-ion battery (mobile cell battery). The sorbent shows high selectivity for Li(I) against Co(II), Mn(II), Ni(II), Fe(III) and Al(III) ($SC_{Li/Metal}$: 26–85); much lower against Cd(II) (i.e., 2.3).

Keywords:
The sulfonation of chitosan strongly enhances the recovery of lithium from aqueous solutions Uptake kinetics are fitted by the pseudo-first- order rate equation and sorption isotherms by the Langmuir dual site equation
Lithium sorption remains highly selective for Li (I) against alkali-earth and heavy metals High stability in performances of sorption and desorption for eighteen cycles
At pH 2.2 sulfonated chitosan selectively recovers lithium from acidic leachate of mobile phone Li-ion battery (for sustainable valoriza-tion of strategic metal)

1. Introduction

In the last decade (apart its historical use in ceramic, glass manufacture and aluminum production), the "explosive" development of rechargeable batteries for electronics, hybrid and electric vehicles has driven the demand for lithium to unexpected levels [1]. The global consumption of lithium-ion batteries for automotive applications is expected to represent a business of about 220 US billions from 2015 to 2024 [2]. Currently, the conventional production of lithium comes from brine and mineral resources. About 80% of mining resources (production and reserves) is identified in a limited number of countries (Australia, China, Chile, Canada and Argentina) [1,3]. These strategic issues as well as the increasing demand may explain the strong incentive politics of national and regional regulations for developing the recycling of waste and spent equipment, including for lithium, though no significant industrial production from secondary resource has been reported for Li. The rate of recycling of Li from spent materials is actually evaluated to less than 10% [3].

The composition of Li-ion battery makes these spent materials a remarkable "alternative" as mining resource. Indeed, Gerold et al. [1] compiling the literature gave average composition of Li-ion battery as: 5–7% Li, 5–20% Co, 5–10% Ni and a certain variety of complementary heavy metals accounting for 5–10% (including Cu, Al, Fe, Cr, etc.). After the separation of plastic-based cartridges, and the pre-treatment of spent

* Corresponding authors.
E-mail addresses: yzwei@usc.edu.cn (Y. Wei), eric.guibal@mines-ales.fr (E. Guibal).

batteries (though grinding, magnetic and densimetric separations), the solid is usually submitted to acidic leaching (as for the processing of mineral resources) [4–6]. A large variety of techniques may be used for the treatment of Li-ion battery (or ore) leachates and brines, and the recovery of valuable metals including:

(a) precipitation [7,8],

(b) crystallization [9],

(c) solvent extraction [10–12],

(d) ion-exchange [13–17] (including ion-exchange membranes, [18]), or.

(e) chelating resin [19,20].

The choice of the treatment process (including combined techniques) strongly depends on the composition of the leachates, the relative concentrations of valuable metals, and the process strategy (purification of Li leachates by removal of co-metals [16,21] or direct removal of lithium). The complexity of Li-containing effluents makes the selectivity a critical challenge in the design of sorbent. Alexandratos et al. [22] immobilized crown-ethers onto polymer supports for developing Li-selective sorbents. Among ion-exchange resins, Arroyo et al. [14] compared different types of reactive groups for Li(I) sorption: iminodiacetic reactive groups (Lewatit TP 207 and 208 resins) and sulfonic acid groups (Lewatit K2629 resin). The sorption levels from brines (under weakly acidic solutions) range between 0.17 and 0.38 mmol Li g^{-1}. Güneysu [15] demonstrated that at near-neutral pH the weakly cationic Lewatit CNP 80 resin (acrylic acid-based resins) is more efficient for Li (I) sorption than strong acidic Armfield resin. Xu et al. [23] reported the synthesis of sulfonated cellulose microspheres (activated with glycidyl methacrylate) and applied this new sorbent for Li(I) sorption at mild pH (around 6–8). Volkova et al. [24] discussed the order of affinity for Li(I) of a series of cation-exchange resins bearing sulfonic groups (KU 2–8, Purolite C100, and Resinex KW-8), carboxylic groups (SG-1, Purolite C104FL, and Resinex KW-H) and phosphoric groups (Purolite S957). While comparing the distribution coefficients of Li and other impurities (Na, K, Mg Ca and Fe cations) at different pH values, they conclude that carboxylic-based resins are highly efficient for separating alkali metals from lithium (not sorbed), at pH 2–3. On the other hand, the preferential sorption of alkali-earth metals (compared with lithium) by sulfonic-based resins makes these sorbents efficient for purifying mixed solutions at pH 2.

These different results oriented the current research towards the development of sulfonic-bearing sorbents for Li(I) recovery from solutions of increasing complexity (synthetic pure solutions → multi-component synthetic solutions → acidic leachates of Li-ion batteries).

Herein, the strategy for the design of the new sorbent is based on the functionalization of chitosan (aminopolysaccharide commercially produced by deacetylation of chitin, major constituent of crustacean shells). Chitosan bears amine groups that can be used for metal sorption by chelation at near-neutral pH of metal cations through free electron-doublet on N, or by ion-exchange/electrostatic attraction of metal anions on protonated amine groups (in acidic solutions) [25]. These amine groups can be used for the functionalization of the biopolymer and for its shaping (preparation of hydrogels, foams, membranes, and so on). The high density of hydroxyl groups (responsible of its hydrophilic behavior) also offers possibilities for grafting new functional groups; this is precisely the strategy used for the sulfonation of chitosan in this work (Sulfo-C). The sorption properties of Chito (glutaraldehyde-crosslinked chitosan) and Sulfo-C micro-particles for Li(I) are widely investigated (study of pH effect, uptake kinetics, sorption isotherms at different temperatures, selectivity and competition effects). The desorption of lithium from loaded sorbents and the recycling are carried out. Finally, Sulfo-C is tested for the recovery and separation of Li(I) from a complex solution (acidic leachate of Li-ion phone cell battery). In parallel, the sorbent is characterized by a series of techniques to characterize both the structure of the sorbent and its interactions with Li(I).

The work described for the first time the sulfonation of chitosan using an original procedure involving a specific sulfating agent (synthesized by reaction of sodium nitrite and sodium hydrogen sulfate, under reflux). This method is cost-effective and does not require complex reagents, or hazardous solvent (as mentioned in most of the available literature). The study will illustrate the outstanding sorption properties (compared with conventional Li(I) sorbent), the remarkable stability of the sorption and desorption properties, the fast kinetics for metal sorption, and the effectiveness of the sorbent for the recovery of target metal from complex (synthetic or industrial) effluent containing several competitor ions.

2. Materials and methods

2.1. Materials

Chitosan (acetylation degree, DA, close to 25%), glutaraldehyde solution (25% w/w) as well as $NaHSO_3$ (>99.9%), NaOH (≥97.0%), and $NaNO_2$ (≥99.0%), $LiNO_3$ (used for most sorption tests) and LiCl (≥99.98%) (used for salinity and selectivity tests) were provided by Sigma Aldrich (Merck KGa, Darmstadt, Germany). Sodium chloride (≥99.98%), $MgCl_2{\cdot}6H_2O$ (99%), $AlCl_3{\cdot}6H_2O$ (95%), $FeCl_3$ (≥99.5%), $ZnCl_2$ (≥99.5%), $NiSO_4$ (≥99.8%) were obtained from Guangdong Guanghua, Sci-Tech Co., Ltd (Guangdong, China). Calcium chloride (≥99.1%) (used for selectivity tests) was purchased from Shanghai Makclin Biochemical Co., Ltd. (Shanghai, China).

2.2. Sorbent synthesis and characterization

Scheme S1 (Supplementary Information) shows the different steps in the synthesis of both Chito and Sulfo-C sorbents. Detailed descriptions of the synthesis procedures are reported in Supplementary Information (Section A). Briefly, chitosan sorbent (Chito) was produced as glutaraldehyde cross-linked biopolymer, as the reference material (support, SI, Section A.1). The functionalized sorbent (i.e., Sulfo-C) was obtained by a two-stage process. A sulfating agent ($N(SO_3Na)_3$) was first synthesized (SI, Section A.2). This intermediary product was reacted with chitosan (in solution) under controlled thermal conditions (85 °C) before processing the glutaraldehyde crosslinking (under reflux) and the precipitation in alkaline conditions (SI, Section A.3). Scheme 1 shows the structures of Chito and Sulfo-C sorbents. The methods used for the characterization of the materials are reported in Section B.1 (Supplementary Information).

2.3. Sorption and desorption studies

2.3.1. Sorption tests

Sorption tests were performed in batch systems using a reciprocal shaker at fixed agitation speed (i.e., 210 rpm). A fixed volume of solution (V, L) containing a given amount of metal ion (i.e., C_0, mmol Li L^{-1}) was mixed with a fixed amount of sorbent (m, g). The pH was adjusted to target value using either HNO_3 or NaOH molar solutions. Though the pH was not controlled during the sorption step, the equilibrium value was systematically monitored at equilibrium. After fixed values of contact times (for kinetics) or after 24/48 h, samples were collected and filtrated before being analyzed for assessing residual metal concentrations (C_{eq}, mmol L^{-1}). The mass balance equation was used for calculating the sorption capacity (q_{eq}, mmol Li g^{-1}): $q_{eq} = (C_0\text{-}C_{eq}) \times V/m$.

The precise experimental conditions are systematically reported in the caption of the Figures. Experiments were systematically duplicated and shown in Figures (for illustrating the good reproducibility of sorption tests).

2.3.2. Desorption studies

For the study of metal desorption, the metal-loaded sorbents (which were collected from previous kinetic or equilibrium experiments) were mixed for given contact times with an eluent solution (0.2 M HCl solution). The sorbent dose (SD) was set to 2 g L^{-1} for desorption. For sorbent

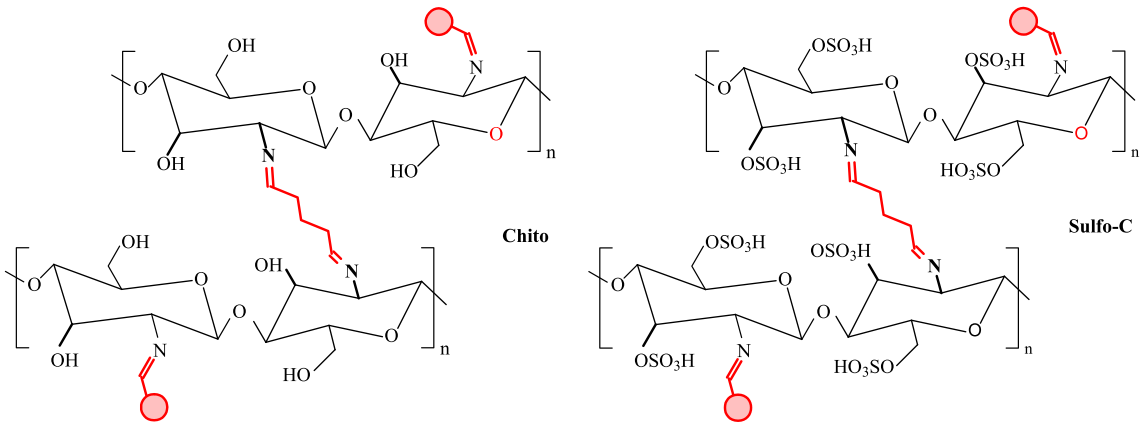

Scheme 1. Suggested structures for Chito and Sulfo-C sorbents.

re-use, the sorbent was rinsed several times with water between each operating step. The sorbed Li amounts at the different steps and in the eluate (for desorption step) were compared to calculate the loss in sorption efficiency and the effectiveness of metal desorption.

In the case of sorbent loaded with multi-component solutions, several types of eluents were tested (including hydrochloric, sulfuric, acetic, oxalic acids and EDTA, 0.2 M) in order to evaluate the possibility to separate these metal ions not only during the sorption step but also at the desorption stage. The sorbent dose was: 0.2 g L^{-1} (other experimental conditions: v: 210 rpm; time: 2 h).

2.3.3. Modeling of sorption

Conventional equations were used for modeling uptake kinetics and sorption isotherms. The relevant models are summarized in Table S1 (see Supplementary Information, SI). The determination of model parameters was derived from non-linear regression analysis (using the facilities of Mathematica®). The quality of the fits was analyzed by comparison of experimental and calculated data using the determination coefficient (i.e., R^2) and the Akaike Information Criterion (AIC; lower values researched, and differences significant when $|\Delta AIC|>2$).

2.4. Application to the treatment of acidic leachate of waste Li-ion battery

2.4.1. Leaching

Different types of Li-ion mobile batteries were used for the application test (phone cell batteries as in Figure S1). The batteries were dismantled and the plastic parts were discarded. After grinding to 0.5 mm size, the material was quartered. The sample (0.5 g) was mineralized in a Teflon beaker at 110–160 °C using a series of acids. Concentrated HF acid was used for Si digestion (S/L ~ 1:10). In a second step, after evaporation, a mixture of HNO_3 and HCl (1:3 M ratio; volume: 20 mL) was added in the presence of hydrogen peroxide (1.5–2 mL; 32%, w/w) for the dissolution of organic electrolyte. After complete dissolution (total volume: 10 mL); the solution was diluted with demineralized water into a 100-mL volumetric flask for analyzing metal content. Table S2 reports the metal contents in the Li-ion battery (powder).

The batteries were grinded and the powder (particle size range around 1 mm) was initially mixed for 2 h with 5 M HCl solution, at T: 100 °C (in a closed reactor). The velocity of agitation was set to 150 rpm. The solid/liquid (S/L) ratio was fixed to 1:3 (50 g for 150 mL). In order to enhance the leaching of the metals from the battery, a few drops of concentrated HCl and H_2O_2 were progressively added to the mixture (final HCl concentration ≈7 M). The leachate was collected for processing Li(I) sorption using Sulfo-C sorbent. The volume of leachate collected was 125 mL.

2.4.2. Processing of leachates

The effect of pH on metal sorption was tested in the range pH_{eq}: 1–3.8. The selectivity in metal recovery was measured both for as-produced leachates and for oxalic acid-completed leachates (1% oxalic acid solution, w/w). The sorbent dose was 1 g L^{-1}, T: 20 ± 1 °C, and the contact time: 10 h.

3. Results and discussion

3.1. Summary of the characterization of sorbents

The detailed physicochemical characterization of the sorbents is discussed in section B (in SI). Herein, main characterizations are summarized. The particle size (sieving and SEM observation) allows fixing the average particle size close to 20 ± 5 μm (Figure S2). The textural analysis shows that the functionalization of crosslinked chitosan increases the specific surface area from 9 to 27 m^2 g^{-1} (with relevant increase of porous volume) (Section B.2.1., Figure S3). The study of thermal degradation of Chito and Sulfo-C sorbents shows 3 and 4 transitions steps (respectively) with a global weight loss that decreases from 88.5% to 80.3 % after sulfonation of Chito (Section B.2.2., Figure S4).

The effective grafting of sulfonate groups is clearly demonstrated by elemental analysis (Table S3): while N content hardly changes between Chito and Sulfo-C, the functionalized sorbent contains S element (1.27 mmol S g^{-1}; with simultaneous increase in O content, as RSO_3^- moiety). This chemical modification is also characterized by FTIR analysis (Section B.2.3., Table S4, Figures 1 and S5). The sulfonation shifts the large band at 3400 to 3421 cm^{-1} (corresponding to the overlapping of NH and OH stretching vibrations). The C=O ester stretching vibration (at 1729 cm^{-1}) almost disappears; this is followed by the enlargement of the Amide I band (C=O stretching at 1646 cm^{-1}, which is shifted to 1621 cm^{-1}). The reinforcement of C-N stretching appears on the 1418 cm^{-1} band (shifted to 1451 cm^{-1}), while several bands representative of S-based vibrations appear after modification; meaning doublet at 633 and 590 cm^{-1} for sulfonate groups, 1261 cm^{-1} (-S=O), 1161 and 607 cm^{-1} (sulfonamide), 788 cm^{-1} (C-O-S stretching), and 527 cm^{-1} (C-S). The X-ray photoelectron spectroscopy also contributes to demonstrate the efficiency of sulfonation as appearing in Fig. 2 (survey XPS curve). Figures S6-S9 show the high resolution XPS spectra for selected signals for Chito and Sulfo-C before and after Li(I) sorption; Table S5 suggests the assignment of the different deconvoluted bands appearing in Figures S6-S9. Section B.2.4. (in SI) provides detailed discussion of these spectra and characterizes the appearance of sulfonate groups (though the discussion of S *2p* signals and the changes observed on C *1s* and O *1s* signals, due to the modification of their chemical environment): appearance of new deconvoluted bands and little shifts in their binding energies.

At the macroscopic scale, the chemical functionalization of Chito sorbent is also confirmed by the shift in the pH_{PZC} values of Sulfo-C (from 6.38 to 4.8 after sulfonation) (Section B.2.5., Figure S10). It is

noteworthy that the same titration (pH-drift) method allows observing a new decrease of the pH_{PZC} of Sulfo-C after Li(I) sorption, while after metal desorption (including after 5 cycles of sorption/desorption) the titration curve almost overlaps with the initial curve (as a proof of the macroscopic stability of the sorbent).

3.2. Chemical characterization of Li(I) interactions with sorbents

3.2.1. FTIR characterization

The sorption of Li(I) from acidic acid solution may involve substantial changes in the FTIR spectra due to the shifts of bands associated with the protonation of some reactive groups and to the direct interaction of some reactive groups with Li cations (Fig. 1). Hence, the sorption of lithium induces the shift of the 3421 cm^{-1} band to 3446 cm^{-1} probably due to the protonation of amine groups and to Li(I) binding with amine groups. The changes observed in the region 1640–1620 cm^{-1} confirm the contribution of amine/amide groups. A series of strong bands are observed after Li(I) sorption:

(a) the broad band in the range 1350–1100 cm^{-1}, and.

(b) the bands at 800 cm^{-1} (C-O-C of the polysaccharides and nitrate ions from the medium [26]), 662 cm^{-1} (broad band that may include N-O contribution, from nitrate), 606 cm^{-1} (associated with C-S and C-O-S stretching vibrations), and 445 cm^{-1} (for polysulfide (S-S) stretching [26]).

These changes result from shifts of existing bands and formation of new vibrations associated with the modification of the environment of amine and sulfonate reactive groups (due to protonation and/or interactions with Li cations). In order to verify the proper effect of sorbent protonation on its spectrum, Figure S5 compares the spectra of the Sulfo-C as-produced, after being in contact with water at pH_0 2, and after Li(I) sorption (also at pH_0 2). Table S4 also reports the assignments of the different bands. Most of the shifts observed after Li(I) sorption are also reported for the protonated sorbent (Sulfo-C(P)). The most significant differences (which could be more precisely attributed to Li-sorbent interaction) correspond to:

(a) the band at 3422 cm^{-1} for Sulfo-C(P) (comparable to raw sorbent) and lower than in the case of Li-loaded sorbent (at 3446 cm^{-1}),

(b) the band appearing at 1621 cm^{-1} in Sulfo-C, shifted to 1628 cm^{-1} for Sulfo-C(P) and to 1637 cm^{-1} after metal binding; this band is assigned to C=O stretching vibration (Amide I band),

(c) the band at 1418 cm^{-1} in Sulfo-C, shifted to 1429 cm^{-1} for Sulfo-C(P) and up to 1438 cm^{-1} after Li(I) uptake; the C-N stretching vibration is affected by metal binding (modification of C-N chemical environment).

(d) the weak band at 1161–1157 cm^{-1} for sorbent (raw and protonated) is replaced with a strong and broad band shifted to 1188 cm^{-1} after Li(I) binding (which overlaps other signal present in this region on the sorbent); sulfonamide and S=O groups are involved in Li(I) binding.

(e) the new bands appearing at 446 cm^{-1} and 416 cm^{-1} (with high intensity) after metal binding can be assigned to polysulfide-type band (appearing as a small signal at 467 cm^{-1} on protonated sorbent). This is probably due to the tautomeric effect that displaces some bonds to form this polysulfide-based compound. The same mechanism of acidic tautomerization can explain the formation of the band at 445 cm^{-1} for the sorbent analyzed after fives cycles of sorption and desorption.

After metal desorption, the FTIR spectrum of the sorbent is partially restored. The main differences concern the broad band at 3444 cm^{-1} (not restored to 3421 cm^{-1}). The desorption is operated with 0.2 M HCl solution (and water rinsing), which does not allow turning back to Sulfo-C FTIR spectrum. The other FTIR region that is substantially different from original Sulfo-C spectrum concerns the broad band initially present at 1621 cm^{-1}; this band is replaced with a doublet at 1737 cm^{-1} and 1634 cm^{-1}. These bands (well-resolved) are probably associated with carbonyl groups (1737 cm^{-1}) and protonated amine groups (1634 cm^{-1}). The intermolecular rearrangements resulting from tautomerization and acidic conditions (associated with elution step) induce formation of carbonyl bands as shown by the appearance of the band at 1737 cm^{-1}, but also the broadening and increase in intensity of the band at 1164 cm^{-1} (which may be assigned to sulfonamide group). Therefore the changes observed in these regions are probably more associated with the protonation of the sorbent than to the direct interactions with Li(I) (which, apparently, concern more specifically the broad band 1350–1100 cm^{-1} and the band at 662 cm^{-1}).

3.2.2. XPS characterization

Figures S8 and S9 show the high resolution XPS spectra of the sorbents after lithium binding (as a complement to XPS survey curve, Fig. 2). Table S5 summarizes the assignments of the binding energies (BEs) for selected signals (and their atomic percentages, At.%) for the sorbents before and after metal binding. After Li(I) sorption, the signals are also strongly affected. The weak sorption of Li(I) onto Chito leads to poorly resolved Li *1 s* signal appearing as a single peak at BE: 55.5 eV (assigned to Li form). The sulfonation enhances metal sorption, and the relevant signal is considerably more intense; in addition, the deconvolution of the signal shows two components at BE: 55.9 eV and 58.1 eV, assigned to Li-N and Li-SO_3, respectively. The signals for N *1* s are affected with the appearance of a specific band at BE 400.4 eV (N-Li) and the decrease in intensity of the other N bands. In the case of Sulfo-C, a new component for O *1* s band appears at 530.0 eV associated with O-Li bond (in sulfonate environment). The other components are slightly shifted in BE, and relative atomic percentages (At., %): substantial increase in the contribution of O-N and strong decrease in the intensity of the O-S bond. This confirms that both amine groups and sulfonic groups are involved in lithium uptake with Sulfo-C sorbent. On the opposite

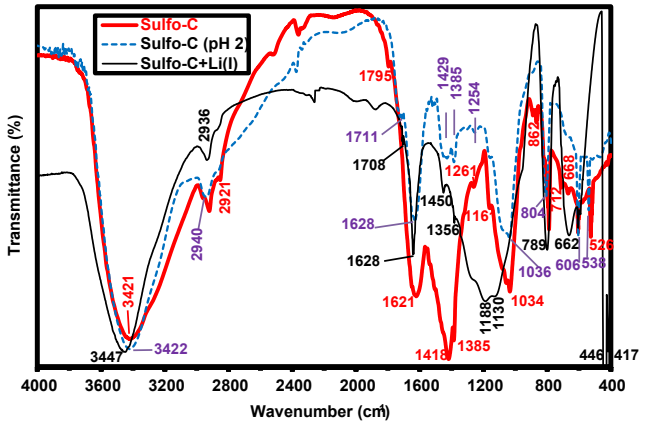

Fig. 1. Comparison of the FTIR spectra of Sulfo-C (raw), Sulfo-C (after contact with pH_0 2 solution), and Sulfo-C after Li(I) sorption at pH_0 2.

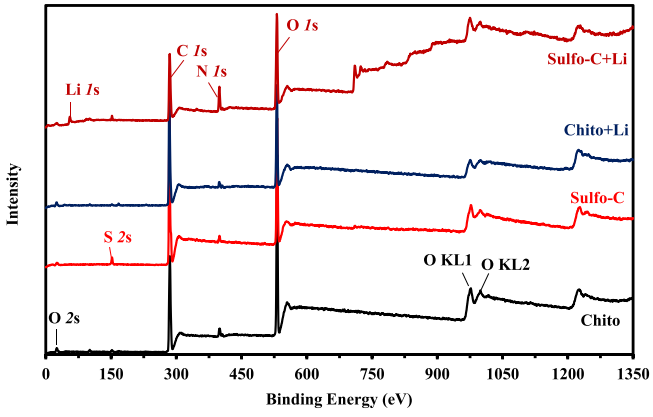

Fig. 2. XPS survey of sorbent before and after Li(I) sorption.

hand, for Chito only the signals associated to amine groups and (N-based moieties) are involved in lithium binding. Section B.2.4 (in SI) provides a detailed discussion of these characterizations.

3.3. Li(I) sorption properties

3.3.1. Effect of pH

Fig. 3 compares the pH effect on Li(I) sorption using both Chito and Sulfo-C. Duplicate experiments confirm the experimental reproducibility and the stability in sorption performances (especially for Sulfo-C, in the complete pH range). The sulfonation of the precursor (i.e., Chito) strongly improves the maximum sorption capacity from ≈1.8 mmol Li g^{-1} to ≈12 mmol Li g^{-1}. The optimum pH for the two sorbents is close to 2–2.5. It is noteworthy that for Sulfo-C the sorption capacity strongly increases with the pH between 1 and 2 and sharply decreases with the pH above pH 3. It is also remarkable that the lowest sorption capacities at pH ≈1 and pH ≈5.5 remain in the range 1–2 mmol Li g^{-1} (i.e., comparable to the highest q_{eq} values for Chito). In the case of Chito, the sorption capacity weakly decreases above the optimum (i.e., pH 2–2.5): from 1.8 to 1.4 mmol Li g^{-1}. The weaker impact of pH for Chito sorbent is probably associated to the highest value of pH_{PZC} that maintains the surface of the sorbent positively-charged. In strongly acidic solutions (i.e., pH 1), the competition of protons limits the sorption of Li^+. Above pH 3, the protonation of the surface of Sulfo-C progressively decreases, which, in turn, may limit the ion-exchange of Li cation with protonated reactive groups of the sorbent. Sulfonic groups are more affected by deprotonation effect than amine groups; this may explain that at pH 5.5 Sulfo-C maintains sorption capacity at relatively high level (same order of magnitude than Chito). Fig. 3 also shows the effect of pH on Li(I) sorption at a higher temperature (i.e., 50 ± 1 °C). The optimum pH is not influenced by the temperature, remaining close to 2–2.5. However, the maximum sorption capacity significantly decreases at T: 50 °C compared with 20 °C: 8.2 *vs.* 11.7 mmol Li g^{-1}. This is a first indication of the exothermic nature of Li(I) sorption. Physical sorption is frequently associated with exothermic characteristics.

Figure S11a and Section C.1. (in SI) show that the pH hardly varies with metal sorption. The slope of the $\log_{10}$ plot of the distribution ratio ($D = q_{eq}/C_{eq}$, L g^{-1}) *vs.* pH_{eq} significantly varies with the sorbent (Figure S11b). The slope for Sulfo-C is close to + 1; this is consistent with the ion-exchange of one proton with one Li^+. On the opposite hand, for Chito the slope is reduced (close to + 0.38); the sorption mechanism is different (consistently with FTIR and XPS characterizations).

3.3.2. Uptake kinetics

The kinetic profiles are compared in Fig. 4 for Chito and Sulfo-C. The superposition of duplicate curves confirms the reproducibility of sorption tests. The equilibrium is reached within 60–90 min at T: 20 °C. This

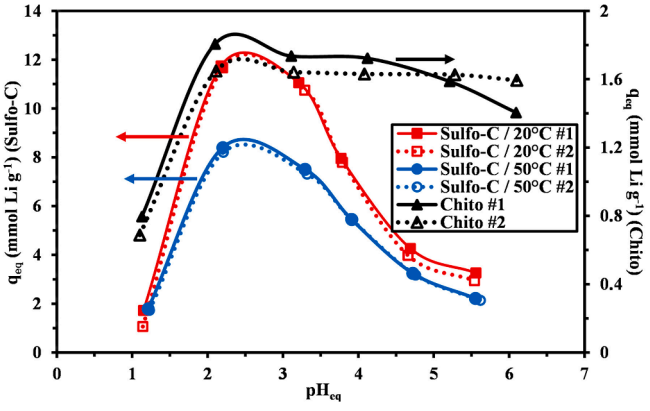

Fig. 3. Effect of pH on Li(I) sorption using Chito and Sulfo-C sorbents (Sorbent dose, SD: 0.4 g L^{-1}; Time: 48 h; v: 210 rpm; T: 20 ± 1 °C).

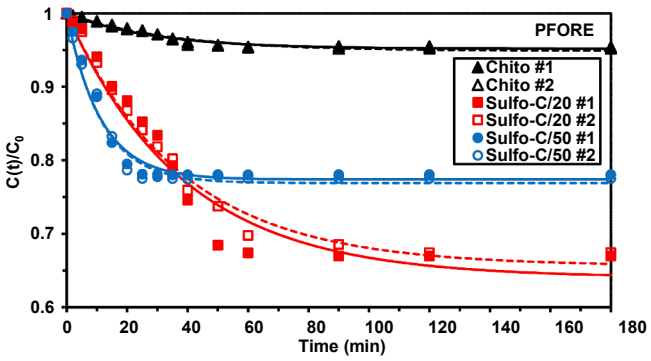

Fig. 4. Uptake kinetics for Li(I) removal using Chito and Sulfo-C sorbents at pH_0 2 (including temperature effect on lithium sorption onto Sulfo-C) – Modeling with the PFORE (C_0: 15 mmol Li L^{-1}; SD: 0.4 g L^{-1}; v: 210 rpm).

equilibrium time is relatively long, taking into account the small size of sorbent particles (i.e., 20 ± 5 μm). Ones would expect faster sorption for micron-size sorbents where the diffusion path is limited to 10 μm-length. This means that the resistance to intraparticle diffusion, which is one of the possible limiting steps, may play a non-negligible role in the overall control of uptake kinetics. The agitation rate was set to 210 rpm, based on preliminary studies that showed fine dispersion of particles and negligible effect of resistance to bulk and film diffusion. The other mechanism that may control uptake kinetics is the proper reaction rate of sorption, which can be described by pseudo-first and pseudo-second order rate equations (Table S1a). Fig. 4 also reports the uptake kinetics for T: 50 °C in the case of Sulfo-C sorbent (under similar experimental conditions). Consistently with Fig. 3, the equilibrium concentration is higher than that at T: 20 °C, because the sorption is exothermic. However, the equilibrium is reached within a shorter contact time (i.e., ≈30 min). The thermal activation globally enhances the mass transfer characteristics (probably by improvement of diffusional movements inside the sorbent) or the proper reaction rate.

Table 1 summarizes the parameters of the three models (PFORE, PSORE and RIDE). Based on both R^2 and AIC values, the kinetic profiles are better fitted by the PFORE. In Fig. 4, the lines represent the fits of experimental profiles with the PFORE (PSORE and RIDE fits are reported in Figure S12). The calculated values for q_m slightly overestimate the experimental values of the sorption capacity at equilibrium (actually by less than 10 %, meaning much less than PSORE). As expected from experimental profiles, the apparent kinetic rate (i.e., k_1) are of the same order of magnitude for Chito and Sulfo-C at T: 20 °C, in the range 2.58–3.47 × 10^{-2} min^{-1}, while for T: 50 °C k_1 is almost tripled (8.94–8.75 × 10^{-2} min^{-1}). Simonin [27] and Hubbe et al. [28] published comprehensive analyses of the literature dedicated to the discussion of kinetic modeling. They both commented that in most cases the PSORE model is abusively assigned to chemisorption because of inappropriate selection of experimental conditions or processing of data. More specifically, this model corresponds, in many cases (involving inappropriately designed experimental conditions), to systems controlled by the resistance to intraparticle diffusion.

Despite the poor fitting of experimental profiles (especially in the zone of high curvature) by the RIDE (i.e., Crank equation), the effective diffusivity coefficient is used here for comparing the systems and as a confirmation of the contribution of resistance to intraparticle diffusion in the control of uptake kinetics. Indeed, D_e values are close to 7.8–6.7 × 10^{-13} m^2 min^{-1}, 4.7–4.5 × 10^{-13} m^2 min^{-1}, and 1.8–1.7 × 10^{-12} m^2 min^{-1} for Chito (at T: 20 °C), Sulfo-C at T: 20 °C, and Sulfo-C at T: 50 °C, respectively. These values are several orders of magnitude lower than the molecular diffusivity of lithium in water (i.e., 6.17 × 10^{-8} m^2 min^{-1}, [29]). This is another confirmation that the resistance to intraparticle diffusion cannot be neglected in the control of the kinetics of lithium sorption. The thermal activation favors the Brownian diffusion in the

Table 1
Modeling of uptake kinetics for Li(I) removal using Chito and Sulfo-C sorbents.

	Sorbent		Chito		Sulfo-C			
	Temperature		20		20		60	
Model	Parameter	Run #	1	2	1	2	1	2
Exp.	$q_{eq.exp.}$		1.685	1.800	12.2	12.2	8.09	8.45
PFORE	$q_{eq.1}$		1.770	1.916	13.2	12.9	8.32	6.68
	$k_1 \times 10^2$		3.47	2.96	2.58	2.64	8.94	8.75
	R^2		0.968	0.981	0.962	0.990	0.982	0.979
	AIC		−170	−177	−107	−128	−131	−130
PSORE	$q_{eq.2}$		2.175	2.409	17.1	16.5	9.36	9.75
	$k_2 \times 10^3$		16.3	11.9	1.36	1.50	12.8	12.2
	R^2		0.942	0.960	0.939	0.975	0.940	0.939
	AIC		−163	−168	−102	−118	−116	−116
RIDE	$De \times 10^{13}$		7.79	6.69	4.69	4.55	18.1	17.5
	R^2		0.947	0.961	0.933	0.971	0.959	0.958
	AIC		−160	−162	−96	−108	−118	−118

Units: q, mmol g^{-1}; k_1, min^{-1}; k_2, g $mmol^{-1}$ min^{-1}; D_e, m^2 min^{-1}.

sorbents, and the global mass transfer (though at the expense of lower sorption capacities).

3.3.3. *Sorption isotherms and thermodynamic parameters*

The sorption isotherms summarize the distribution of the solute between liquid and solid phases at equilibrium for increasing concentrations, under the same experimental conditions (including pH and temperature). Fig. 5 shows the comparison of sorption isotherms at pH 2 for Chito (at T: 20 °C) with the profiles for Sulfo-C at T: 20, 30, 40, and 50 °C. Again, the good superposition of experimental curves demonstrates the reproducibility of sorption tests. As expected from previous results, the sorption efficiency strongly increases with the sulfonation of the precursor, and significantly decreases with the increase of the temperature for Sulfo-C. The superiority of Sulfo-C may be explained by acid-base properties (Section 3.1), the diversity, and reactivity of functional groups (Section 3.2.). Lithium is classified among the hard acids according the HSAB principles [30]. Therefore, the cation has a marked preference for hard bases (i.e., higher affinity for O-bearing ligands than N-bearing ligands).

The experimental profiles have been modeled using the Langmuir, the Freundlich, the Sips, and the Temkin equations. Table 2 reports the Freundlich parameters for the sorption isotherms, while those values for the other equations are summarized in Table S6. The comparison of R^2 and AIC values allows discarding the Langmuir, Sips and Temkin equations; Figure S13 shows the Langmuir fits of experimental profiles, which fail to correlate the isotherms in the highly-curved sections. This conclusion may be partly explained by the fact that the saturation of the sorbents is not reached even with a residual concentration as high as 60–68 mmol Li L^{-1}. The power-type expression of the Freundlich equation accounts for the unsaturated shape of the isotherm. Another explanation may be associated to the coexistence of two types of reactive groups, as observed through the study of interaction modes (Section 3.2.). In order to address this hypothesis, the Langmuir Dual Site (LDS) equation was tested for fitting experimental data [31]:

$$q_{eq} = \frac{q_{m1} \times b_1 \times C_{eq}}{1 + b_1 \times C_{eq}} + \frac{q_{m2} \times b_2 \times C_{eq}}{1 + b_2 \times C_{eq}} \quad (1)$$

where (q_{m1}, b_1) and (q_{m2}, b_2) are the Langmuir parameters for sorption sites S1 and S2, respectively (with mmol g^{-1} and L $mmol^{-1}$ units, respectively).

The parameters and the statistical indices are reported in Table 2 (together with Freundlich modeling, Fig. 5a). Though the LDS equation fits less accurately the experimental profiles than the Freundlich equation, the quality of the correlation is globally better than with those of the other equations. Fig. 5b displays the LDS fitting of experimental profile. The coexistence of different reactive groups with different affinity for Li(I) is illustrated by the large variation in the b_{Li} coefficients. The sites S_1 are characterized by high $q_{m,L1}$ values and very low b_{L1}, while the sites S_2 show lower $q_{m,L2}$ values (2–3 times) but much higher affinity coefficients than for S_1 sites (85–244 times). S_1 sites are probably associated with amine groups, while S_2 sites are assigned to sulfonic groups (almost irreversible/rectangular isotherm). Section C.2. (in SI) reports complementary analysis of the effect of temperature on the relative contributions of the two types of reactive group; apparently the contribution of amine groups increases with temperature (Figures S14-S15).

Tran et al. [32] recently commented that the Freundlich constants cannot be used for calculating thermodynamic parameters using the van't Hoff equation due to the inappropriateness of units. Herein, the van't Hoff equation was individually applied to the two terms of the Langmuir dual site equation (i.e., b_{L1} and b_{L2}). Lima et al. [33] pointed out the importance to convert the affinity coefficient of the Langmuir equation to make it dimensionless before applying the van't Hoff equation [32].

$$\Delta G^{\circ} = -RT\ln K^0_{Eq} \quad (2a)$$

$$\Delta G^{\circ} = \Delta H^{\circ} - T\Delta S^{\circ} \quad (2b)$$

$$\ln K^0_{Eq} = -\frac{\Delta H^{\circ}}{RT} + \frac{\Delta S^{\circ}}{R} \quad (2c)$$

$K_{eq}{}^0$ is the standard thermodynamic equilibrium constant (dimensionless), where in the case of Langmuir equation gives:

$$K^0_{eq} = b_L \times \frac{C^0_{Li}}{\gamma_{Li}} = b^0_{L,i} \quad (2d)$$

With $C_{Sorbate}{}^{\circ}$ (1 mol L^{-1}) and $\gamma_{Sorbate}$ (dimensionless) are the unitary standard concentrations of sorbate and the activity coefficient of sorbate in solution, respectively. Frequently, in the studies on sorption processes, the concentration range is limited enough to consider that the activity of the sorbate is close to the unity. The maximum residual concentration in Fig. 5 reaches 70 mmol Li L^{-1}; this makes the approximation inappropriate. The activity coefficient was evaluated close to 0.874 (using Eq. (2e)).

$$\ln(\gamma_{Li}) = -0.509 z^2_{Li}\sqrt{I}, with I = \frac{1}{2}\sum_i z_i^2 c_i \quad (2e)$$

$$\ln\left(b_L \times \frac{C^0_{Li}}{\gamma_{Li}}\right) = -\frac{\Delta H^{\circ}}{RT} + \frac{\Delta S^{\circ}}{R} \quad (2f)$$

The enthalpy changes are systematically negative as a confirmation of the exothermic nature of Li(I) sorption onto Sulfo-C (Table 3). In addition, the order of magnitude of ΔH° is relatively low (i.e., −13/-21 kJ mol^{-1}), meaning that the uptake proceeds through physisorption. The entropy changes are also systematically negative: the global randomness of the system decreases with Li(I) sorption and the sorption

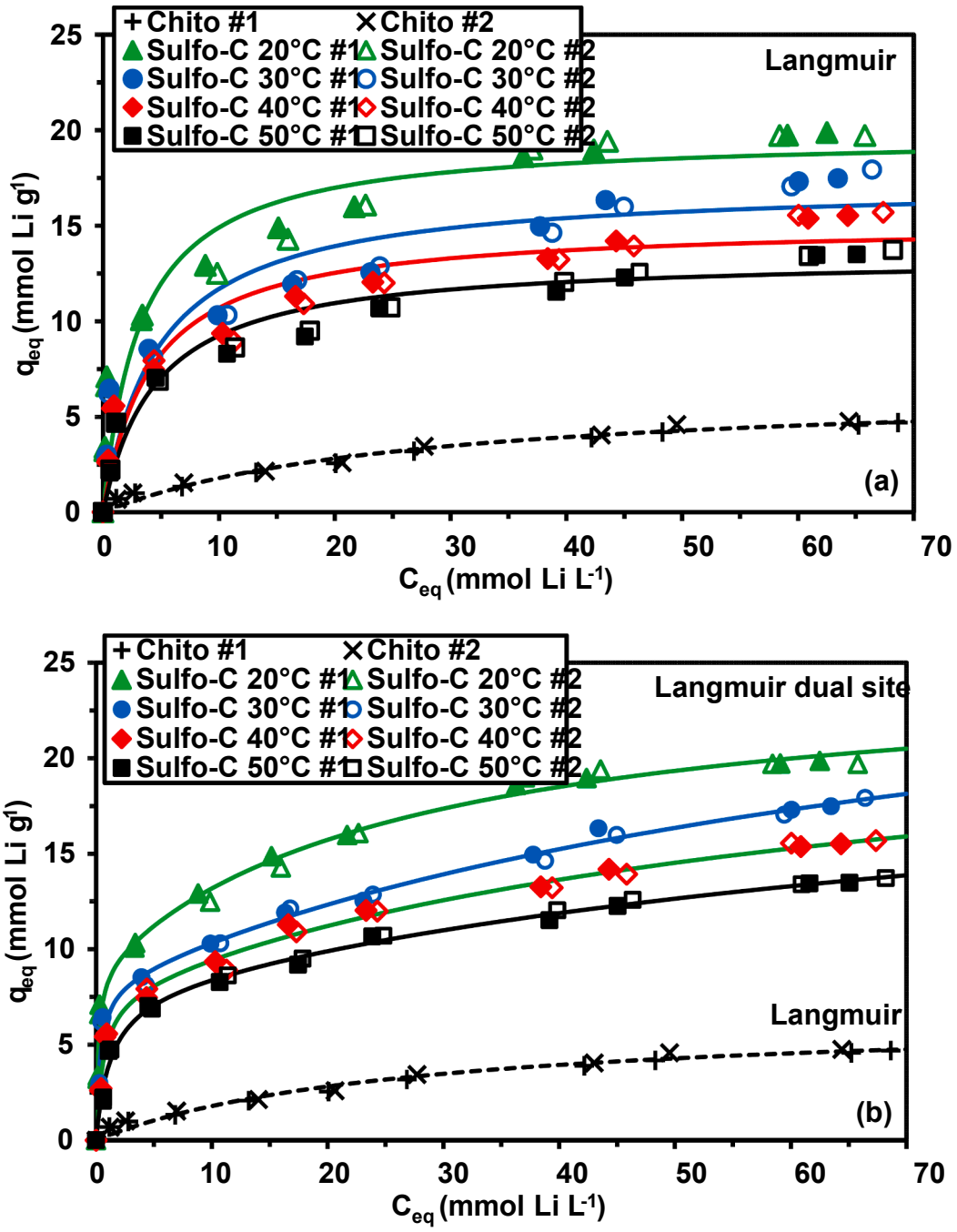

Fig. 5. Modeling of Li(I) sorption isotherms at pH 2 using Chito and Sulfo-C sorbents using Freundlich equation (a) and Langmuir dual site equation (b) (SD: 0.4 g L^{-1}; time: 48 h; v: 210 rpm; T: 20 ± 1 °C; pH_{eq}: 2–2.13 for Chito and 2.2–2.3 for Sulfo-C; in (b) panel the Langmuir equation is applied for Chito instead of Langmuir dual site equation).

is enthalpy-driven.

Table 4 compares the sorption properties of Chito and Sulfo-C sorbents with alternative sorbents recently characterized in the literature. The functionalized sorbent is ranked among the most efficient, at least in terms of maximum sorption capacity although the affinity coefficient (b_L) remains relatively low compared with, for example, Lewatit TP207 [14], MnO_2 and ion sieves [34,35] or spinel $Li_4Mn_5O_{12}$ sorbent [36]. It is noteworthy that most of the existing literature focuses on Li recovery from neutral or alkaline solutions; this makes the strict comparison relatively difficult since the current work considers lithium sorption from acidic solutions (i.e., pH 2). The closest experimental conditions (at pH 3 and above) were reported by Cicek et al. [19] using an aminomethylphosphonic resin: the maximum sorption capacity reached 2 mmol Li g^{-1} and the affinity coefficient was reported close to 0.0003 L $mmol^{-1}$; i.e., significantly lower than the values reported for Sulfo-C.

3.3.4. *Sorption mechanism*

The different data collected from FTIR and XPS analyses (and pH_{PZC} determination), the study of pH effect leads to the identification of different modes of interaction with Li(I) cations. Indeed, the coexistence of free amine groups (and hydroxyl groups) and sulfonic groups (grafted onto the biopolymer) opens the possibility for lithium to interact with NH_2 groups (XPS analysis showed that amine groups are not totally engaged in crosslinking with GA), –OH, and $–SO_3H$. XPS analysis

Table 2
Modeling of Li(I) sorption isotherms using Chito and Sulfo-C sorbents at pH_0 2 – Parameters of Freundlich and Langmuir dual site equations (only for Sulfo-C sorbent).

	Sorbent	Chito	Sulfo-C			
	Temperature	20 °C	20 °C	30 °C	40 °C	50 °C
Model	Parameter					
Experiment	$q_{m,exp.}$	4.87	19.86	17.92	15.69	13.72
Freundlich	k_F	0.608	7.73	5.62	4.89	4.07
	n_F	2.03	4.28	3.68	3.59	3.43
	R^2	0.991	0.984	0.986	0.990	0.987
	AIC	−78	−26	−28	−44	−38
Langmuir dual site	$q_{m,L1}$		15.9	21.6	16.2	15.1
	$b_{L,1}$		0.0371	0.0121	0.0145	0.0099
	$q_{m,L2}$		9.04	8.25	7.79	7.85
	$b_{L,2}$		5.51	2.956	1.693	0.843
	R^2		0.992	0.991	0.994	0.993
	AIC		−14	−17	−31	−28

Units: Units: q, mmol g^{-1}; b_L, (L $mmol^{-1})^{nS}$; n_S, dimensionless; k_F, $mmol^{1-1/nF}$ $L^{1/nF}$ g^{-1}; A_T, L mol^{-1}; b_T, J kg $mmol^{-2}$.

Table 3
Thermodynamic parameters for Li(I) sorption using Sulfo-C sorbent at pH_0: 2 – Individual contributions of Sites S_1 and S_2 (deduced from Langmuir dual site modeling).

Sites	S_1			S_2		
Parameter	ΔH°	ΔS°	ΔG°	ΔH°	ΔS°	ΔG°
20	−13.08	−32.1	−3.05	−21.12	−40.4	−8.48
30			−2.73			−8.07
40			−2.41			−7.77
50			−2.09			−7.26
R^2	0.715			0.996		

Units: ΔH° and ΔG°, kJ mol^{-1}; ΔS°, L mol^{-1} K^{-1}.

showed also that the environments of O-bearing and N-bearing groups are affected by lithium binding (O-Li, and N-Li signals). The interactions of lithium with sulfonic groups may involve direct ion-exchange mechanism but also interactions associated with the tautomerization of sulfone groups. This is also shown in the FTIR analysis through (a) the decrease of the relative intensity of OH and NH groups and/or (b) shifts in the wavenumbers following lithium sorption. Since the sorption is enhanced at pH lower than the full deprotonation of the sorbent, this means that the cation exchange properties of the sorbent are engaged in Li^+ uptake (via Li^+ exchange with H^+ from OH, NH and SO_3H groups) and tautomerization of available π bonds of sulfonic moieties. Scheme 2 shows tentative modes of interaction between functional groups and lithium cation.

3.3.5. *Competitor effects and sorption selectivity*

The sorption performance may be affected by the complexity of the solution, including the effect of ionic strength. A very abundant literature deals with lithium recovery from brines [14,37]. Figure S16 focuses on the impact of NaCl on the sorption properties of Li(I) using Sulfo-C. The optimum pH remains close to 2–2.5 (Figure S16a); however, the sorption capacity progressively decreases with the concentration of the salt: from 11.7 mmol Li g^{-1} (as the reference) to 4.57 mmol Li g^{-1} in 5 M (Na,Cl) solution. The strong impact of ionic strength is frequently associated with ion-exchange mechanisms. In seawater, the Na,Cl salt concentration is around 0.5 mol kg^{-1}, the sorption capacity (at pH ≈2) for 1 M Na,Cl solution remains as high as 10.87 mmol Li g^{-1} (loss lower than 7%). This means that the sorbent remains highly selective against Na^+ (even with an excess as large as 63 times). In Figure S16b, the distribution ratio, $D = q_{eq}/C_{eq}$ (L g^{-1}), linearly varies with the concentration of Na,Cl in the solution (or ionic strength of the solution, neglecting the contribution of $LiNO_3$).

Complementary tests were performed on multi-component equimolar solutions (i.e., 1 mmol L^{-1}), at different pH values for optimizing the selectivity of Li(I) sorption using Sulfo-C sorbent. The selectivity coefficient ($SC_{Li/Me}$) for Li(I) against other metal ions is defined as the quotient of distribution ratios:

$$SC_{Li/Me} = \frac{D_{Li}}{D_{Me}} = \frac{q_{Li} \times C_{Me}}{C_{Li} \times q_{Me}} \quad (3)$$

Fig. 6a reports the SC values for Li against selected competitor metal cations for different pH values. On the opposite hand, Fig. 6b reports the separation properties for the same system with the addition of oxalic

Table 4
Comparison of Li sorption properties of Chito and Sulfo-C with literature.

Sorbent	pH	time	$q_{m,exp.}$	$q_{m,L}$	b_L	Ref.
Ion-sieve	8	1440	–	3.75	148	[34]
Ca-alginate beads	7	1440	0.031	0.081	3×10^{-5}	[41]
K-birnessite	5–7	60	0.332	0.399	0.0024	[42]
MnO_2 ion-sieve	10	-[a]	3.05	3.13	32.6	[35]
Spinel $Li_4Mn_5O_{12}$	9.74	600	0.859	0.815	139.5	[36]
Polyacrylamide/MnO_2 ion-sieve	10.1	1800	2.64	2.95	8.60	[43]
Spinel $H_{1.1}Li_{0.08}Mn_{1.73}O_{4.05}$	12	720	–	7.20	0.00085	[44]
Imprinted crown ether/macroporous membrane	9	150	3.96	4.35	0.417	[45]
Aminomethylphosphonic resin	> 3	15	–	1.97	0.0003	[19]
Multi-wall carbon nanotube	6	30	–	2.00	0.059	[46]
Ion-imprinted mesoporous sorbent	7	240	1.80	2.32	5900	[47]
Lewatit K2629 (sulfonic) resin	7.84[b]	30	–	0.265	0.750	[14]
Lewatit TP207 (imino-diacetic acid) resin	7.84[b]	30	–	0.366	16.9	[14]
Photo-responsive Li-ion imprinted polymer/C_3N_4	7	30	3.28	7.30	0.035	[48]
Ti-intercalated $LiMnO_2$ composite	[c]	5760	–	3.16	0.347	[49]
Mo-doped/TiO_2 sieve	12[d]	1200	11.5	12.0	0.0212	[50]
$H_4Mn_5O_{12}$ nanotubes	12	120	5.33	5.43	0.887	[51]
Spinel $LiMn_2O_4$ nanofiber	11	1440	4.97	4.81	2.46	[52]
K marxianus yeast	9	5	–	0.788	0.389	[53]
Sulfonated cellulose beads	10	60	2.31	2.31	–	[54]
Phosphorylated hazelnut shell	5.8	6	0.792	1.11	0.402	[55]
Chito	2	90	4.87	6.58	0.037	*This work*
Sulfo-C	2	120	19.9	19.9	0.284	*This work*

[a] : fixed-bed column experiment;
[b] : sea-water reverse osmosis brine;
[c] : Li-spiked sea-water;
[d] : simulated brine;

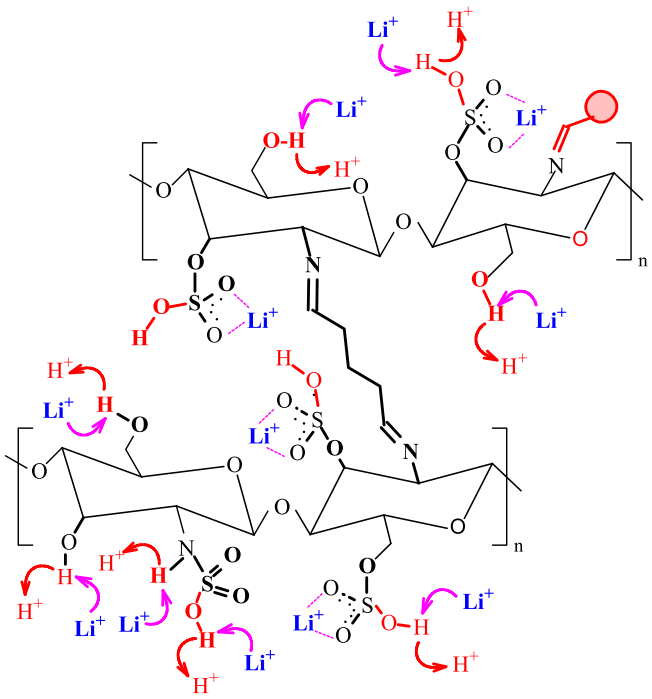

Scheme 2. Tentative mechanisms of Li(I) sorption onto Sulfo-C.

acid (at 1% concentration, w/w). Indeed, the addition of oxalic acid was frequently reported for improving the separation of Li(I) from other cations [16,38,39]. This is explained by the preferential complexation of heavy metals by oxalate (compared with lithium).

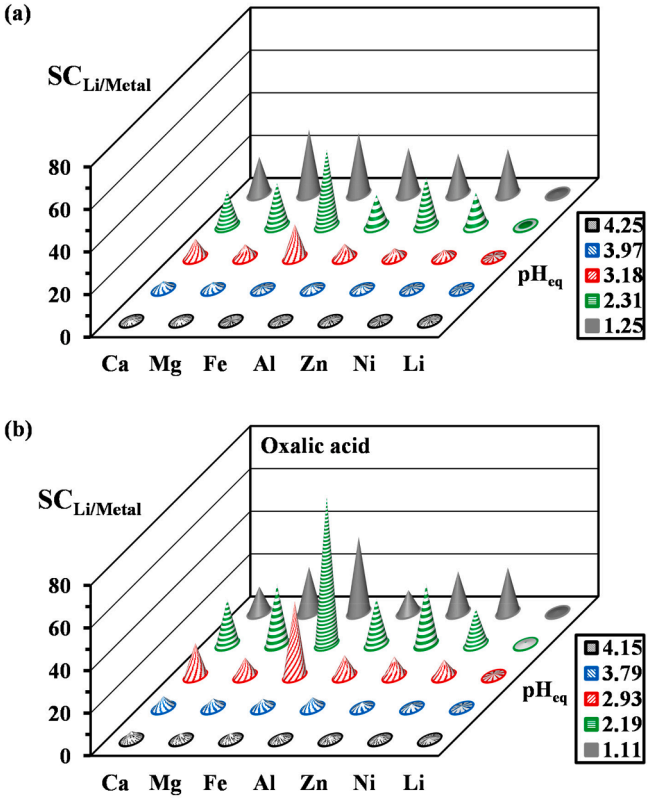

Fig. 6. Effect of pH on the selectivity coefficient ($SC_{Li/metal}$) for metal sorption from multi-component equimolar concentrations using Sulfo-C sorbent – without (a) and with oxalic acid (1%, w/w) (b) (C_0: 1 mmol L^{-1}; SD: 1 g L^{-1}; Time: 10 h; v: 210 rpm).

The $SC_{Li/Me}$ values are strongly influenced by the equilibrium pH. Consistently with the high sensitivity of Li(I) removal to the pH (optimum sorption at pH 2–2.5 for Sulfo-C), the highest selectivity for Li against other metals is obtained at pH close to 2. The selectivity at pH 2 (in absence of oxalic acid) may be ranked according to:

Fe(III) (35.8) ≫ Zn(II) (22.7) > Mg(II) (20.0) > Ca(II) (16.4) > Ni(II) (15.4) > Al(III) (14.4).

In the presence of oxalic acid, the selectivity slightly increases (except for Fe(III) where the $SC_{Li/Fe}$ is almost doubled) but the ranking is weakly affected (larger variations reported for Ca(II), Al(III) and Ni(II)):

Fe(III) (69.3) ≫ Zn(II) (28.2) ≈ Mg(II) (28.1) > Al(III) (21.4) ≈ Ca(II) (20.9) > Ni(II) (16.6).

The presence of oxalate that complexes metal cations limits their availability for being sorbed onto Sulfo-C and their ionic affinity for binding groups (especially sulfonic groups). Therefore, the competitor effect of these cations is reduced and the selectivity coefficient for Li(I) increases with the presence of oxalic acid; this is more specifically observed for Fe(III) ≫ Mg(II) > Zn(II) > Al(III) ≈ Zn(II) ≫ Ca(II) ≫ Ni (II), consistently with the ranking of the stability constant of metal-oxalate complexes [40].

Section C.3. (in SI) shows complementary analysis of competition effects (including the variation of distribution ratios with pH, Figure S17). This allows clearly illustrating the optimum separation of Li (I) from other cations at pH 2. Some correlations are also reported (in Figures S18-S19) between the selectivity coefficients and the intrinsic physico-chemical properties of metal ions (Table S7). These SC values cannot be directly correlated to specific criteria; however, the metals were grouped (as doublets) regarding their respective impacts on competitor effect mainly through criteria such as hydrated radius and solution-phase electronegativity.

3.3.6. *Metal desorption and sorbent recycling*

Figure S20 compares the kinetic profiles for Li(I) using 0.2 M HCl solution for Chito (loaded at T: 20 °C) and Sulfo-C (loaded at T: 20 °C and 50 °C). The eluent is highly efficient: lithium is completely desorbed within 30 min of contact (under selected experimental conditions). It is noteworthy that the desorption kinetics is significantly faster for Sulfo-C sorbent loaded at T: 20 °C than for the other systems; indeed, 15 min are sufficient for total metal desorption.

Fig. 7 compares the sorption and desorption efficiencies for Chito and Sulfo-C along 15 and 18 successive re-use cycles, respectively. First, for the two sorbents, the desorption remains highly efficient (around 100%) at each step, using 0.2 M HCl solution. The comparison of the sorption efficiencies shows that for Sulfo-C the performance remains remarkably stable: the loss remains close to 10% at the 18th cycle, contrary to Chito that loses about 43% at the 15th cycle. Surprisingly,

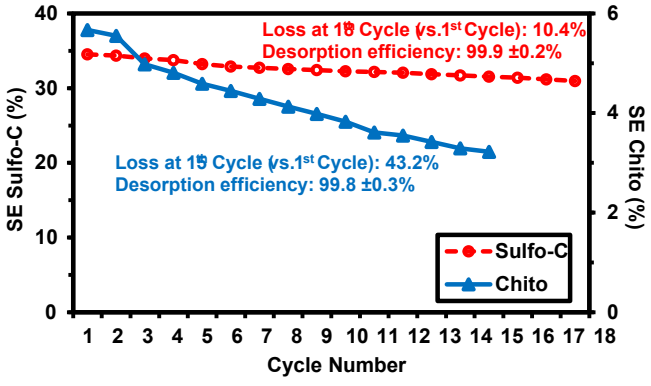

Fig. 7. Sorption and desorption efficiencies for the recycling of Chito and Sulfo-C sorbents for Li(I) recovery (Sorption, C_0: 14.4 mmol Li L^{-1}; SD: 0.4 g L^{-1}; time: 24 h; pH 2 – Desorption, 0.2 M HCl eluent; SD: 2 g L^{-1}; time: 2 h; water rinsing between each step).

the functionalized material reveals remarkably more stable than the precursor, which may be either chemically modified or degraded along recycling steps. Indeed, the stability in desorption performance means that the loss in sorption efficiency is not associated with the accumulation of the metal onto the sorbent (and its progressive saturation).

Section C4 (in SI) compares different eluents for testing the possibility to separate the metals through specific desorption. None of the tested eluents succeeds in separating the metals loaded on Sulfo-C (samples collected from studies on multi-component equimolar solutions) (Figure S21). Hydrochloric acid solution is the most efficient (but non-selective). Oxalic acid is highly efficient for releasing competitor ions (due to complexing effect) but not selectively (10% of lithium is co-desorbed).

3.4. Application to metal recovery from waste battery

3.4.1. Acidic leaching

Table S2 shows the composition of the acidic leachate, which is characterized by the presence of three major elements: Li (≈40.0%), Al (≈30.9%), and Fe (≈22.2%), counting for 93.1% of total metal content. Valuable traces are constituted of Co (≈2.5%), Ni (≈1.9%). The remaining (≈2.5%) is formed of other heavy metals. Compared with the contents of metals in the batteries (as derived from the analysis of mineralized batch), these data show that:

(a) Li extraction exceeds 90%,

(b) Fe (the most abundant heavy metal in Li-ion batteries) is weakly leached (around 60%),

(c) other heavy metals are efficiently leached (efficiency varies between 88% and 98%).

3.4.2. Treatment of acid leachate

Figure S22 reports the effect of pH on the sorption capacities of Sulfo-C for selected metals in absence (Fig. S22a) and presence of oxalic acid (Fig. S22b). Consistently with their relatively high proportions in the leachates, the highest sorption capacities are reported for Li(I)≫Fe(III)≈Al(III)≫>≫Co(II) > Mn(II) > Ni(II) > Cd(II) in absence of oxalic acid. The introduction of oxalic acid slightly changes the ranking for the trace elements according Li(I)>>Al(III)≈Fe(III)>>>Ni(II) > Co(II) > Mn(II) ≈Cd(II). It is noteworthy that consistently with the sensitivity of Li(I) sorption onto Sulfo-C to pH, the sorption capacity reaches a maximum at pH_{eq} 2–2.5, while for the other elements the sorption capacity continuously increases with pH. Obviously, derived from these results, the highest selectivity for Li(I) recovery is obtained in this specific pH range (i.e., pH 2–2.5). This conclusion is confirmed by Fig. 8. The highest $SC_{Li/metal}$ values are systematically obtained at pH_{eq} 2.28 (in absence of oxalic acid) according: Al(III)(85.7) >> Fe(III)(60.6) > Ni(II)(56.4) > Mn(II) (53.0) >> Co(II)(26.5) >> Cd(II)(10.6). The introduction of oxalic acid changes the order of selectivity coefficients at pH_{eq} 2.17 according: Fe (III)(74.6) ≈ Al(III)(72.8) >> Co(II)(34.7) > Mn(II)(27.0) >> Ni(II) (9.7) >> Cd(II)(2.6). It is noteworthy that the presence of oxalic acid moves the optimum pH value for the separation of Li(I) from Co(II) to pH 1.07 ($SC_{Li/Co}$ reaches 61.4). Table S8 summarizes the values of the main criteria (i.e., C_{eq}, sorption efficiency, q_{eq} and distribution ratio) for the different metal ions at pH_{eq} ≈ 2.2. Oxalic acid enhances the sorption properties of Sulfo-C for Cd(II), Ni(II) and Mn(II) (to a lesser extent). On the other hand, the recovery of Co(II), Mn(II), and Li(I) is slightly reduced (while Al(III) is hardly affected). These trends are comforted by the plots of the concentration factor ($CF = q_{eq}/C_0$, L g^{-1}) appearing in Figure S23. These data allow observing:

(a) optimum concentrating effect of Li(I) at pH 2–2.5 (greater without oxalic acid), the concentrating effect increases with the pH for other metals,

(b) the second metal showing the highest concentrating effect is Cd (II),

(c) the presence of oxalic acid reinforces the concentrating effect of Ni(II) (and slightly reduces the values of CF for the other metal ions).

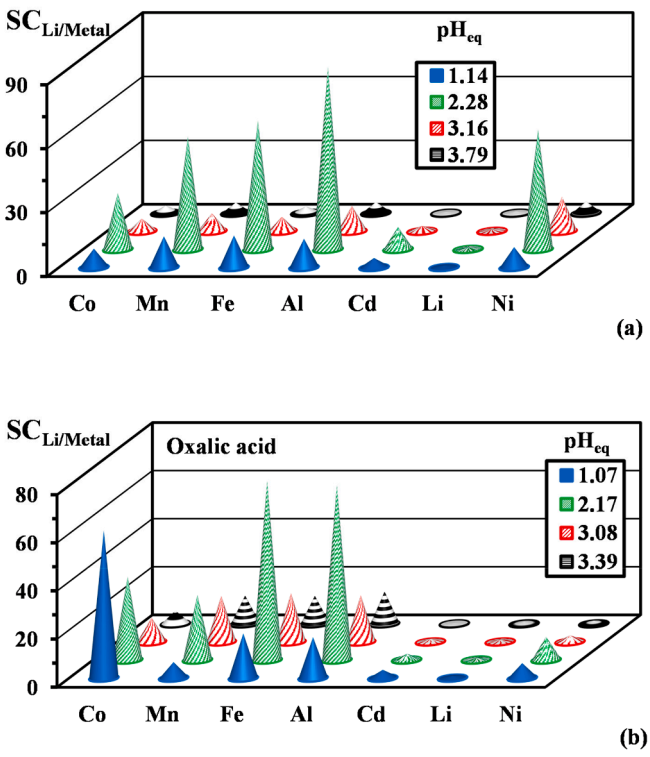

Fig. 8. Effect of pH on the selectivity coefficient ($SC_{Li/metal}$) for metal sorption from battery leachate using Sulfo-C sorbent – without (a) and with oxalic acid (1%, w/w) (b) (SD: 1 g L^{-1}; Time: 10 h; v: 210 rpm).

Section C.5. provides a complementary analysis of cadmium separation from battery leachate, since cadmium shows an atypical behavior compared with other divalent cations (Figures S23-S24). The addition of oxalic acid increases the selectivity of the sorbent for Cd(II) at pH ≈ 3.4 against other divalent cations. However, these conditions do not allow efficiently separating cadmium from lithium.

Despite the complexity of leachate composition (compared with synthetic pure solution – Fig. 7), the sulfonated sorbent shows good stability for Li(I) recovery (and complete metal desorption along 15 cycles) (Fig. 9): the loss in sorption efficiency does not exceed 15% at the 15th cycle. This is a little higher than the loss observed at the 15th step for synthetic pure solution (i.e., 8.6%). The presence of other metal ions

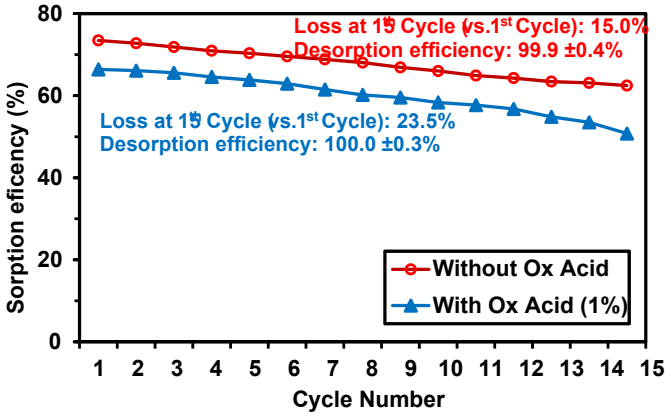

Fig. 9. Sorption and desorption efficiencies for the recycling of Sulfo-C sorbent for Li(I) recovery using Li-ion mobile phone batteries – effect of oxalic acid addition (Sorption, C_0: 9.33 mmol Li L^{-1}; SD: 1 g L^{-1}; time: 5 h; pH 2.28 – Desorption, 0.2 M HCl eluent; SD: 2.5 g L^{-1}; time: 2 h; water rinsing between each step).

may explain this little decrease in sorption performance: lithium desorption being complete, it is possible anticipating that this is mainly due to the binding of competitor metals that may be not fully desorbed. It is noteworthy that the presence of oxalic acid (1%, w/w) decreases the sorption efficiency by 7.6 ± 1.4% (compared with the leachate without oxalic acid); the loss in sorption efficiency increases after the 12th cycle.

4. Conclusion

The characterization of sulfonated chitosan by elemental analysis, FTIR, and XPS spectroscopy clearly shows the effectiveness of the functionalization. The sulfonation drastically increases the sorption of Li (I): from 4.9 mmol Li g^{-1} (for Chito) to 19.9 mmol Li g^{-1} (for Sulfo-C). Apparently both amine groups (weak) and sulfonic groups (strong) are involved in Li(I) binding; this makes the sorption isotherms better fitted by the Freundlich and Langmuir dual site equations. The strong affinity of sulfonate groups for Li(I) is the major contributor to metal sorption, especially at low metal concentration, while amine groups have lower affinity. The sorption is fast; 60 min are sufficient for reaching equilibrium. However, the contribution of resistance to intraparticle diffusion cannot be neglected. The kinetic profiles are fitted by the pseudo-first order rate equation. Increasing the temperature speeds up the kinetics but decreases the sorption capacity. Lithium sorption is exothermic. Metal desorption is highly effective using 0.2 M HCl solutions and the sorption efficiency of Sulfo-C is maintained at high level for at least 18 cycles of sorption and desorption. In acidic solutions (i.e. pH 2–2.5), the sorbent is highly selective for Li(I) against selected alkali-earth and heavy metals; the selectivity is enhanced at this pH when oxalic acid (1%, w/w) is added to the solution. These results are confirmed in the processing of acidic leachates (produced from Li-ion mobile battery). At pH 2–2.5, the sorbent is selective to Li(I) against other heavy metals. At pH ≈ 3.4, the sorbent is selective for both Li(I) and Cd(II); however, the addition of oxalic acid causes in this case a loss in the selectivity of the sorbent for Cd(II) against Ni(II).

Sulfo-C sorbent appears very promising for the recovery of Li(I) from acidic complex solutions such as acidic leachates of batteries. The recycling of Sulfo-C for 12 successive sorption/desorption cycles shows a relatively limited decrease in performances: desorption remains close to 100%, while at the 15th cycle the decrease in sorption efficiency does not exceed 15%. The presence of large excess of NaCl affects the sorption performance; however, the sorbent maintains relatively high capacities even in concentrations of Na,Cl as high as 1 M. This preliminary result shows that the sorbent could be also applied to metal recovery from brines. For practical applications, the small size of micron-size particles would make the processing complex (in terms of solid/liquid separation). Obviously, this limits the application of the sorbent in fixed-bed columns. It would be necessary applying this sulfonation process onto hydrogel chitosan beads. An alternatively could consist in functionalizing magnetic/chitosan composites (for batch processing).

Declaration of Competing Interest

The authors declare that they have no known competing financial interests or personal relationships that could have appeared to influence the work reported in this paper.

Acknowledgements

S. M. A. acknowledges Taif University Supporting Project (TURSP-2020/105). E. G., M. F H., and H.M acknowledge the support of the French Government (Institut Français d'Egypte) and Egyptian Academy of Science & Technology (Science and Technology Development Fund) through the IMHOTEP Program (MetalValor project). W.Y acknowledges the support of National Natural Science Foundation of China [U1967218, and 11975082].

Appendix A. Supplementary data

Supplementary data to this article can be found online at https://doi.org/10.1016/j.cej.2022.135941.

References

[1] E. Gerold, S. Luidold, H. Antrekowitsch, Separation and efficient recovery of lithium from spent lithium-ion batteries, Metals 11 (2021) 1091.
[2] Y. Yang, X. Meng, H. Cao, X. Lin, C. Liu, Y. Sun, Y. Zhang, Z. Sun, Selective recovery of lithium from spent lithium iron phosphate batteries: a sustainable process, Green Chem. 20 (2018) 3121–3133.
[3] RSC, Periodic Table, https://www.rsc.org/periodic-table/, Accessed: 5/10/2021.
[4] P. Meshram, B.D. Pandey, T.R. Mankhand, Extraction of lithium from primary and secondary sources by pre-treatment, leaching and separation: A comprehensive review, Hydrometallurgy 150 (2014) 192–208.
[5] A.A. Nayl, R.A. Elkhashab, S.M. Badawy, M.A. El-Khateeb, Acid leaching of mixed spent Li-ion batteries, Arabian J. Chem. 10 (2017) S3632–S3639.
[6] E. Mossali, N. Picone, L. Gentilini, O. Rodriguez, J. Manuel Perez, M. Colledani, Lithium-ion batteries towards circular economy: A literature review of opportunities and issues of recycling treatments, J. Environ. Manage. (2020), 110500.
[7] A. Alsabbagh, S. Aljarrah, M. Almahasneh, Lithium enrichment optimization from Dead Sea end brine by chemical precipitation technique, Miner. Eng. 170 (2021), 107038.
[8] S. Gu, L. Zhang, B. Fu, X. Wang, J.W. Ahn, Feasible route for the recovery of strategic metals from mixed lithium-ion batteries cathode materials by precipitation and carbonation, Chem. Eng. J. 420 (2021), 127561.
[9] K. Ooi, A. Sonoda, Y. Makita, R. Chitrakar, Y. Tasaki-Handa, T. Nakazato, Recovery of lithium from salt-brine eluates by direct crystallization as lithium sulfate, Hydrometallurgy 174 (2017) 123–130.
[10] V.N.H. Nguyen, M.S. Lee, Separation of Co(II), Ni(II), Mn(II) and Li(I) from synthetic sulfuric acid leaching solution of spent lithium ion batteries by solvent extraction, J. Chem. Technol. Biotechnol. 96 (2021) 1205–1217.
[11] V.C.I. Takahashi, A.B. Botelho Junior, D.C.R. Espinosa, J.A.S. Tenorio, Enhancing cobalt recovery from Li-ion batteries using grinding treatment prior to the leaching and solvent extraction process, J. Environ Chem. Eng. (2020), 103801.
[12] N. Thi Hong, M.S. Lee, A review on the separation of lithium ion from leach liquors of primary and secondary resources by solvent extraction with commercial extractants, Processes 6 (2018) 55.
[13] K.-L. Chiu, W.-S. Chen, Recovery and separation of valuable metals from cathode materials of spent lithium-ion batteries (LIBs) by ion exchange, Sci. Adv. Mater. 9 (2017) 2155–2160.
[14] F. Arroyo, J. Morillo, J. Usero, D. Rosado, H. El Bakouri, Lithium recovery from desalination brines using specific ion-exchange resins, Desalination 468 (2019), 114073.
[15] S. Guneysu, Lithium sorption from aqueous solution with cationic resins, Desalin. Water Treat. 177 (2020) 102–108.
[16] S. Virolainen, T. Wesselborg, A. Kaukinen, T. Sainio, Removal of iron, aluminium, manganese and copper from leach solutions of lithium-ion battery waste using ion exchange, Hydrometallurgy 202 (2021), 105602.
[17] T.S. Volkova, V.V. Rudskikh, Using chelate cationites for the purification of a lithium chloride solution, Theor. Found. Chem. Eng. 55 (2021) 772–777.
[18] D. Ipekci, N. Kabay, S. Bunani, E. Altiok, M. Arda, K. Yoshizuka, S. Nishihama, Application of heterogeneous ion exchange membranes for simultaneous separation and recovery of lithium and boron from aqueous solution with bipolar membrane electrodialysis (EDBM), Desalination 479 (2020).
[19] A. Cicek, O. Yilmaz, O. Arar, Removal of lithium from water by aminomethylphosphonic acid-containing resin, J. Serb. Chem. Soc. 83 (2018) 1059–1069.
[20] B. Koo, L.E. Sofen, D.J. Gisch, B. Kern, M.A. Rickard, M.B. Francis, Lithium-chelating resins functionalized with oligoethylene glycols toward lithium-ion battery recycling, Adv. Sustainable Syst. 5 (2021) 2000230.
[21] M.L. Strauss, L.A. Diaz, J. McNally, J. Klaehn, T.E. Lister, Separation of cobalt, nickel, and manganese in leach solutions of waste lithium-ion batteries using Dowex M4195 ion exchange resin, Hydrometallurgy 206 (2021), 105757.
[22] S.D. Alexandratos, C.L. Stine, R.A. Sachleben, B.A. Moyer, Immobilization of lithium-selective 14-crown-4 on crosslinked polymer supports, Polymer 46 (2005) 6347–6352.
[23] C.X. Xu, T.L. Yu, J. Peng, L. Zhao, J.Q. Li, M.L. Zhai, Efficient adsorption performance of lithium ion onto cellulose microspheres with sulfonic acid groups, Quantum Beam Sci. 4 (2020) 14.
[24] T.S. Volkova, V.V. Rudskikh, K.A. Dzhevello, Influence of pH on distribution coefficients of lithium and impurity elements in sorption, Russ. J. Appl. Chem. 89 (2016) 1642–1646.
[25] E. Guibal, Interactions of metal ions with chitosan-based sorbents: a review, Sep. Purif. Technol. 38 (2004) 43–74.
[26] J. Coates, Interpretation of Infrared Spectra, A Practical Approach, in, Encyclopedia of Analytical Chemistry John Wiley & Sons Ltd, 2006, pp. 1–23.
[27] J.-P. Simonin, On the comparison of pseudo-first order and pseudo-second order rate laws in the modeling of adsorption kinetics, Chem. Eng. J. 300 (2016) 254–263.

[28] M.A. Hubbe, S. Azizian, S. Douven, Implications of apparent pseudo-second-order adsorption kinetics onto cellulosic materials: A review, BioResources 14 (2019) 7582–7626.
[29] Y. Marcus, Ion Properties, Marcel Dekker Inc, New York, NY, 1997, p. 259.
[30] R.G. Pearson, Acids and bases 151 (1966) 172–177.
[31] W. Astuti, A. Chafidz, E.T. Wahyuni, A. Prasetya, I.M. Bendiyasa, A.E. Abasaeed, Methyl violet dye removal using coal fly ash (CFA) as a dual sites adsorbent, J. Environ. Chem. Eng. 7 (2019), 103262.
[32] H.N. Tran, E.C. Lima, R.-S. Juang, J.-C. Bollinger, H.-P. Chao, Thermodynamic parameters of liquid–phase adsorption process calculated from different equilibrium constants related to adsorption isotherms: A comparison study, J. Environ Chem. Eng. (2021), 106674.
[33] E.C. Lima, A. Hosseini-Bandegharaei, J.C. Moreno-Piraján, I. Anastopoulos, A critical review of the estimation of the thermodynamic parameters on adsorption equilibria. Wrong use of equilibrium constant in the Van't Hoof equation for calculation of thermodynamic parameters of adsorption, J. Mol. Liq. 273 (2019) 425–434.
[34] L. Wang, C.G. Meng, M. Han, W. Ma, Lithium uptake in fixed-pH solution by ion sieves, J. Colloid Interface Sci. 325 (2008) 31–40.
[35] L. Liu, H. Zhang, Y. Zhang, D. Cao, X. Zhao, Lithium extraction from seawater by manganese oxide ion sieve $MnO_2.0.5H_2O$, Colloids Surf., A 468 (2015) 280–284.
[36] J. Xiao, X. Nie, S. Sun, X. Song, P. Li, J. Yu, Lithium ion adsorption-desorption properties on spinel $Li_4Mn_5O_{12}$ and pH-dependent ion-exchange model, Adv. Powder Technol. 26 (2015) 589–594.
[37] Q. Luo, M. Dong, G. Nie, Z. Liu, Z. Wu, J. Li, Extraction of lithium from salt lake brines by granulated adsorbents, Colloids Surf., A 628 (2021), 127256.
[38] S. Roobavannan, S. Vigneswaran, G. Naidu, Enhancing the performance of membrane distillation and ion-exchange manganese oxide for recovery of water and lithium from seawater, Chem. Eng. J. 396 (2020), 125386.
[39] A. Verma, D.R. Corbin, M.B. Shiflett, Lithium and cobalt recovery for lithium-ion battery recycle using an improved oxalate process with hydrogen peroxide, Hydrometallurgy 203 (2021), 105694.
[40] A.E. Martell, R.M. Smith, Carboxylic Acids, in: Other Organic Ligands, Springer US, Boston, MA, 1977, pp. 1-171.
[41] D. Song, S.-J. Park, H.W. Kang, S.B. Park, J.-I. Han, Recovery of lithium(I), strontium(II), and lanthanum(III) using Ca-alginate beads, J. Chem. Eng. Data 58 (2013) 2455–2464.
[42] H. Ciftci, C. Er, Solid phase extraction of lithium ions from water samples using K-birnessite with layer-structure material form (KBRLSM), Desalin. Water Treat. 56 (2015) 216–222.
[43] J.-L. Xiao, S.-Y. Sun, X. Song, P. Li, J.-G. Yu, Lithium ion recovery from brine using granulated polyacrylamide-MnO_2 ion-sieve, Chem. Eng. J. 279 (2015) 659–666.
[44] M.H. Sorour, H.A. Hani, M.M.H. El-Sayed, A.A. Mostafa, H.F. Shaalan, Synthesis, characterization and performance evaluation of lithium manganese oxide spinels for lithium adsorption, Egypt. J. Chem. 60 (2017) 697–710.
[45] D. Sun, Y. Zhu, M. Meng, Y. Qiao, Y. Yan, C. Li, Fabrication of highly selective ion imprinted macroporous membranes with crown ether for targeted separation of lithium ion, Sep. Purif. Technol. 175 (2017) 19–26.
[46] Y. Huang, R. Wang, An efficient lithium ion imprinted adsorbent using multi-wall carbon nanotubes as support to recover lithium from water, J. Cleaner Prod. 205 (2018) 201–209.
[47] X. Xu, Y. Li, D. Yang, X. Zheng, Y. Wang, J. Pan, T. Zhang, J. Xu, F. Qiu, Y. Yan, et al., A facile strategy toward ion-imprinted hierarchical mesoporous material via dual-template method for simultaneous selective extraction of lithium and rubidium, J. Cleaner Prod. 171 (2018) 264–274.
[48] Y. Huang, R. Wang, Green recovery of lithium from water by a smart imprinted adsorbent with photo-controlled and selective properties, Chem. Eng. J. 378 (2019), 122084.
[49] T. Ryu, J. Shin, S.M. Ghoreishian, K.-S. Chung, Y.S. Huh, Recovery of lithium in seawater using a titanium intercalated lithium manganese oxide composite, Hydrometallurgy 184 (2019) 22–28.
[50] S. Wang, M. Zhang, Y. Zhang, Y. Zhang, S. Qiao, S. Zheng, High adsorption performance of the Mo-doped titanium oxide sieve for lithium ions, Hydrometallurgy 187 (2019) 30–37.
[51] N. Xu, S. Li, M. Guo, Z. Qian, W. Li, Z. Liu, Synthesis of $H_4Mn_5O_{12}$ nanotubes lithium ion sieve and its adsorption properties for Li^+ from aqueous solution, Chemistryselect 4 (2019) 9562–9569.
[52] S. Choi, G. Hwang, S. Ilyas, Y. Han, N.V. Myung, B.-C. Lee, Y. Song, H. Kim, Inorganic nanofiber as a promising sorbent for lithium recovery, Sep. Purif. Technol. 242 (2020), 116757.
[53] H. Gunan Yucel, Z. Aksu, G.B. Yalcinkaya, S.E. Karatay, G. Donmez, A comparative investigation of lithium(I) biosorption properties of *Aspergillus versicolor* and *Kluyveromyces marxianus*, Water Sci. Technol. 81 (2020) 499–507.
[54] C.X. Xu, T.L. Yu, J. Peng, L. Zhao, J.Q. Li, M.L. Zhai, Efficient adsorption performance of lithium ion onto cellulose microspheres with sulfonic acid groups, Quantum Beam Sci. 4 (2020) 6.
[55] Y.K. Recepoglu, A. Yuksel, Phosphorylated hazelnut shell waste for sustainable lithium recovery application as biosorbent, Cellulose 28 (2021) 9837–9855.